Journal of New Materials for Electrochemical Systems 13, 57-67 (2010)

An Electrochemical Investigation of Potential Metallic Bipolar Plate Materials for PEM Fuel Cells

Yan Wang and Derek O. Northwood*

Department of Mechanical, Automotive, and Materials Engineering, University of Windsor,
401 Sunset Avenue, Windsor, Ontario, Canada N9B 3P4

Received: July 29, 2009, Accepted: August 4, 2009

Abstract: *Increasing attention is being paid to the use of metallic materials as a replacement for non-porous graphite in bipolar plates (BPs) for polymer exchange membrane (PEM) fuel cells. The ideal BP material should demonstrate high values of electrical conductivity, thermal conductivity, corrosion resistance and compressive strength and low values of hydrogen/gas permeability and density. Although metallic materials demonstrate many of those properties, their corrosion resistance can be inadequate, which in turn can lead to unacceptable values of contact resistivity. In this study the corrosion properties of SS316L, SS347, SS410, Al6061 alloy, A36 steel and Ti were investigated in simulated PEMFC anode and cathode environments. SS316L, SS347 and Ti exhibited better corrosion resistance than the other metals. The three metals had similar anodic and cathodic corrosion current densities; the corrosion current was negative in the simulated anode conditions and positive in the simulated cathode conditions. These negative currents arose because of the reaction* $2H^+ + 2e^- \rightarrow H_2$ *on the metal electrode and* $2H_2O \rightarrow 4H^+ + O_2 + 4e^-$ *on the platinum electrode. This did not cause corrosion of the metal surface because the negative currents provide cathodic protection. For the Al6061 alloy, and the A36 steel, the cathodic corrosion current density was much larger than the anodic current density. However, for SS410, the anodic current density is larger. Although SS316L, SS347 and Ti had the better corrosion resistance, they still corroded and metal ions would migrate to membrane and therefore degrade both the membrane and the fuel cell performance.*

Keywords: PEM fuel cell, metallic bipolar plates, corrosion.

1. INTRODUCTION

The polymer exchange membrane fuel cell (PEMFC) is one of the most promising candidates as a power source for transportation and stationary applications. Bipolar plates are key components of a PEM fuel cell. Commercial bipolar plates for PEMFCs are made from non-porous graphite because of a lower contact resistance and higher corrosion resistance [1]. However, because non-porous graphite is brittle, non-porous graphite bipolar plates can not be made very thin. Also, it is difficult to machine non-porous graphite bipolar plates. Therefore, bipolar plates account for about 45% of the total stack cost and about 80% of the total weight, which prevents PEM fuel cells from being widely used [2].

Metals are good candidates for bipolar plates because they have high thermal conductivity, are recyclable and can be easily, and consistently, shaped to accommodate the flow channels [1]. A wide range of metals and alloys are available in many price brackets and many of these metals/alloys can be fabricated in thin sections so as to reduce the total volume and weight of a PEMFC. Given these advantages, many researchers have been developing metallic bipolar plates for PEMFCs in the past 10 years or so.

Stainless steel has been the only uncoated metal that has been extensively researched as a bipolar plate material. Li et al [3] examined the electrochemical corrosion characteristics of a 316 stainless steel in a simulated anode environment. They concluded that 316 stainless steel did not spontaneously passivate in the simulated anode environment. Wang et al [4-6] have researched several stainless steels and they concluded a 349TM stainless steel exhibited superior behavior in a simulated PEMFC environment and would be an excellent candidate material for bipolar plates. Other stainless steels examined included AISI 434, AISI436, AISI441, AISI444, and AISI446. The results suggested that AISI446 had barely acceptable characteristics for use as PEMFC bipolar plates. Wang et al [6] also studied a duplex 2205 stainless steel, the nickel content at which was between that of 349TM and

*To whom correspondence should be addressed: Email: dnorthwo@uwindsor.ca

Table1. Substrates and coatings used for metallic bipolar plates.

Coatings \ Substrate	SS	Al	Ti
TiN[8,9,16]	×		
Electrochemical surface treatment[10]	×		
Polymer coating[11]	×		
Nitridation[12,13]	×		
Gold[14]		×	
SUS316L[15]		×	
Active coating (not specified)[17]			×

AISI446. Both electrochemical polarization and interfacial contact resistance measurements indicated that duplex 2205 stainless steel was a possible bipolar plate candidate. Davies et al [7] evaluated different bipolar plate materials and presented long term fuel cell data for Poco® graphite, titanium, and both SS316 and SS310 stainless steels. The properties of the passive films on the surfaces of SS316 and SS310 stainless steels were markedly different. SS310 exhibited better fuel cell performance and showed no degradation after 1400h testing. Analysis of the passive films indicated that this improved performance for SS310 was related to the decreased thickness of the oxide film.

There has been more research on coated metallic bipolar plates. Li et al [8] investigated the corrosion behavior of TiN coated SS316 in simulated PEMFC environments, i.e. 0.01 M HCl+0.01 Na_2SO_4 solutions bubbled with pure oxygen or hydrogen gases. TiN coatings had much better corrosion resistance and passivity under both simulated conditions. No significant degradation took place in TiN coatings under the typical load conditions of a fuel cell for 4h. Cho el at [9] examined TiN coated SS316 as bipolar plates for PEMFC, and compared it with graphite and a bare SS316. In single cell tests, initial performance and lifetime of the TiN-coated 316 bipolar plates was significantly improved over those of bare 316 bipolar plates even though it was still lower than for graphite bipolar plates. Lee et al [10] subjected 316L stainless steel to an electrochemical surface treatment as bipolar plates. The corrosion tests showed that the corrosion current was reduced to one fourth of the original value. Cunningham et al [11] coated a high carbon content-polymer on SS316 and the coatings showed good corrosion resistance. Wang et al [12, 13] researched thermally nitrided stainless steels. Nitridation for 2h at 1100°C resulted in both good corrosion resistance under simulated cathodic and anodic conditions and low ICR, well over an order of magnitude lower than the untreated alloy. Further, little increase in ICR was observed under passivating polarization conditions. Hentall et al [14] coated gold on aluminum for use as bipolar plates. These plates were used in a fuel cell and during the initial warm-up procedure the data indicated performance very similar to graphite. However, very quickly the performance degraded. El-Khatib et al [15] investigated the corrosion stability of high velocity oxy-fuel (HVOF) spray SUS316L coatings on an aluminium substrate. The HVOF thermal spraying technique provided hard SUS316L coatings with high electrical conductivity. The corrosion rates of the coated plates were about one order of magnitude lower than that of uncoated aluminium, and the rate decreased with increase in the coating thickness. Lee et al [16] investigated the effects of a PVD coating on the corrosion resistance of metallic bipolar plates in a PEM fuel cell. The Al-coated plates had better contact resistance and single cell performance than that of the graphite material at the low voltage and shorter cell life. Hodgson et al [17] used metal based bipolar plates in polymer electrolyte membrane fuel cells with an active coating on titanium to reduce voltage losses due to the formation of passive layers. Lifetimes in excess of 8000h have been achieved and power densities in excess of $1.8kWdm^{-3}$ and $1kWkg^{-1}$ were predicted. Table1 presents a summary of the different types of substrates and coatings that have been investigated for use as bipolar plate materials.

In this study, the corrosion properties of six metals including three stainless steels (SS316L, SS347, and SS410), Aluminium alloy 6061, A36 steel, and Ti were investigated in both the simulated anode and cathode environments of a PEMFC in order to determine their potential application as a bipolar plate material.

2. EXPERIMENTAL DETAILS

2.1. Materials

Six materials, including SS316L (Austenitic), SS347 (Austenitic), SS410 (Martensitic), pure Ti (grade2), Al6061 and A36 steel were examined. Their chemical compositions are given in Tables2 and 3.

The plates were cut into samples of 1.5cmx1.5cm, polished on 240-800 grit silicon carbide grinding papers and micropolished with 1μm diameter alumina, and rinsed with ethanol. An electrical contact was made to one side by means of nickel print. Then the

Table2. Chemical compositions of SS316L, SS347 and SS410 (wt%)

Metal	C	Mn	P	S	Si	Cr	Ni	Mo	Cu	Co	N	Al	Ti	Sn	Ta	Nb	Fe
SS316L	0.021	1.82	0.029	0.01	0.58	16.32	10.54	2.12	0.47	–	0.03	–	–	–	–	–	balance
SS347	0.04	1.58	0.029	0.0002	0.57	17.59	9.62	0.34	0.38	–	0.042	–	–	–	0.01	0.63	balance
SS410	0.135	0.36	0.018	0.001	0.4	12.22	0.21	0.03	0.1	0.01	0.012	0.001	0.001	0.011	–	–	balance

Table3. Chemical compositions of Al6061 and A36 steel (wt%)

Metal	C	Mn	P	S	Si	Cr	Cu	V	Ti	B	Ca	Mg	Zn	Ga	Al	Fe
Al6061	–	–	–	–	0.70	0.18	0.25	–	–	–	–	1.12	0.02	0.02	balance	0.46
A36	0.06	0.12	0.004	0.005	0.09	0.02	0.01	0.003	0.003	0.0001	0.0019	–	–	–	0.047	balance

contact side and the edges of the metal sample were sealed by epoxy resin, leaving one side exposed for the electrochemical measurements.

2.2. Electrochemical testing

A standard three-electrode system was used, in which a platinum electrode was used as the counter electrode and a saturated calomel electrode (SCE) as the reference electrode. A Solartron 1285 potentiostat was used to conduct the corrosion tests. Potentiodynamic tests were conducted at both room temperature and 70ºC in order to compare the general electrochemical behavior of the metals. In these tests, samples were stabilized at the open circuit potential (OCP), then the potential was swept from -0.1VvsOCP to 1.2VvsSCE at a scanning rate of 1mV/s. In order to simulate the anode and cathode conditions, potentiostatic tests were conducted at 70 ºC. The applied potential was -0.1VvsSCE purged with H_2 for the anode conditions and 0.6VvsSCE purged with O_2 for the cathode conditions.

2.3. Optical microscopy

In order to observe any corrosion products on the metals, the surfaces of both non-polarized and polarized samples were examined using optical microscopy. A Buehler optical image analyzer 2002 system was used to determine the corrosion products on the specimens.

3. RESULTS AND DISCUSSION

3.1. Polarization behavior of the metals

Figs.1-6 are the anodic polarization curves for the six different metals in a 0.5M H_2SO_4 solution at both ambient temperature and 70°C. From Fig1 for SS316L, we can see the potentiodynamic polarization curve can be divided into three regions. The first region is the active region from OCP to -0.15V, the second region is the passive region from -0.15 to 0.9V, and the third region is the transpassive region from 0.9V to 1.2V. Comparing the two curves in Fig1, the corrosion current at high temperature (70°C) is larger than that at ambient temperature. Thus, in PEMFC conditions, the corrosion rate is more rapid. Fig2 presents the corrosion curves for SS347. We can see that they have almost the same shape as for SS316L. This is because both of the two stainless steels are austenitic stainless steels and their chemical compositions are very similar. It is well known that the chromium content in a stainless steel determines the corrosion resistance because chromium forms a passive film that can prevent further corrosion. Also, nickel can play an important role in corrosion behavior of stainless steels. Nickel has a FCC crystal structure and nickel additions allow the stainless steel to retain a FCC structure at room temperature. Austenitic stainless steels normally have better corrosion resistance than ferritic and martensitic stainless steels because the carbides can be retained in solid solution by rapid cooling from high temperature [18].

Fig3 presents the corrosion curves for SS410. At ambient temperature, SS410 has three areas: an active area, a passive area and a transpassive area. At high temperature (70°C), SS410 has no passive region since SS410 does not form a dense film to prevent corrosion at high temperatures.

Fig4 presents the corrosion curves for Al6061. There is no passive area in these curves. The corrosion current for Al6061 is large, being about 10^{-4}A/cm^2 at ambient temperature and 10^{-3}A/cm^2 at high temperature (70°C).

Fig5 presents the corrosion curves for A36. The corrosion current density can reach values as high as 0.1A/cm^2. From Fig6, we can see that Grade2 Ti has good corrosion resistance because in the potentiodynamic tests, the current density is maintained at a very small value till 1.2VvsSCE at 70°C.

Figs 7 and 8 compare the corrosion resistances of the different metals at ambient temperature and high temperature (70°C), respectively. At ambient temperature, SS316L, SS347, SS410 and Ti exhibit very small corrosion currents in the passive area. The corrosion currents of Al6061 and A36 steel are very high. At the high temperature (70°C), SS316L, SS347 and Ti all have a good corrosion resistance. The other metals are readily corroded.

3.2. Corrosion in simulated anode and cathode conditions

In order to study the potential metallic bipolar plate materials in PEMFC working conditions, corrosion tests were conducted in the simulated anode and cathode conditions of a PEMFC. The simulated anode and cathode tests were -0.1VvsSCE purged with H_2 and 0.6VvsSCE purged with O_2. Since the corrosion potential for the six metals is from -0.2V to -0.7VvsSCE, both the anode and cathode simulated corrosion tests are anodic polarization tests for all six metals.

Fig 9 presents the corrosion curves for SS316L in the simulated anode and cathode conditions. At the cathode, the corrosion current density gradually decreases and stabilizes at $8x10^{-6}$A/cm^2. At the anode, the corrosion current decreases and becomes negative after about 100 seconds. This is in agreement with Wang et al's results on AISI446 [5]. The current density is maintained at about -1×10^{-5}A/cm^2. From Fig 10, we can see the corrosion behavior of SS347 in the simulated anode and cathode conditions. In the anode condition, the corrosion current is -6×10^{-6}A/cm^2 after 120 seconds. The corrosion current is 7×10^{-6}A/cm^2 in the cathode conditions. Comparing the curves for SS316L and SS347, we can see that they have almost the same corrosion behavior. This is because both the chemical composition and structure of these two metals are similar. Fig 11 shows us the corrosion behaviour of SS410. The anodic corrosion current is 2.5×10^{-2}A/cm^2 and the cathodic corrosion current is 4×10^{-3}A/cm^2. In the anode corrosion, the current density suddenly dropped to -0.4V after 1000 seconds because the applied potential can not be maintained at -0.1V. Fig 12 presents the corrosion current densities for Al6061 in the simulated anode and cathode conditions. At the anode, the corrosion current is 4×10^{-3}A/cm^2 after 1 hour and at the cathode, the corrosion current is $1.5x10^{-2}$/cm^2, and after about 1000 seconds, the current density drops to 4×10^{-3}A/cm^2. Fig 13 shows the corrosion current densities for A36 steel. The anodic current density is 5×10^{-3} A/cm^2 and the cathodic current density is 2.5×10^{-2}A/cm^2. We can see that the current density drops suddenly for the anode of SS410 and the cathode of both Al6061 and the A36 steel. After the current density drops, it remains at about 4×10^{-3}A/cm^2. The corrosion current density is large for the anode of SS410 and the cathode of both Al6061 and the A36 steel. Therefore, the corrosion reaction is first controlled by electrochemical polarization. After 1000 seconds, it is controlled by concentration polarization and there are insufficient H^+ ions to maintain a high current. Thus, the applied potential is reduced, and

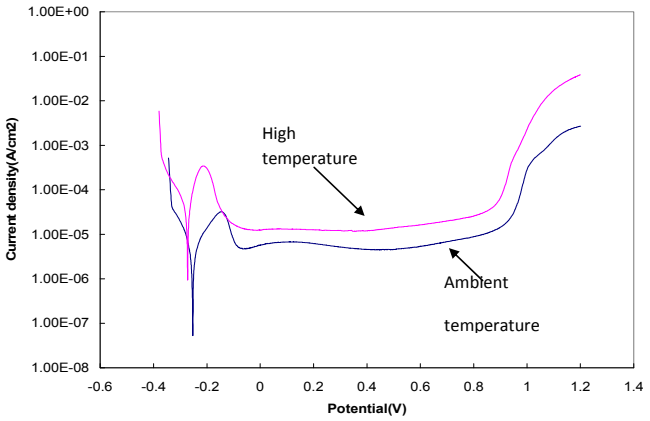

Figure 1. Potentiodynamic polarization curves of SS316L at ambient temperature and 70°C.

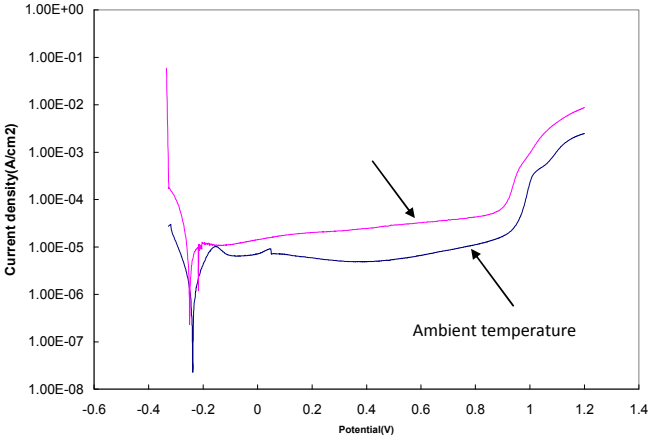

Figure 2. Potentiodynamic polarization curves of SS347 at ambient temperature and 70°C.

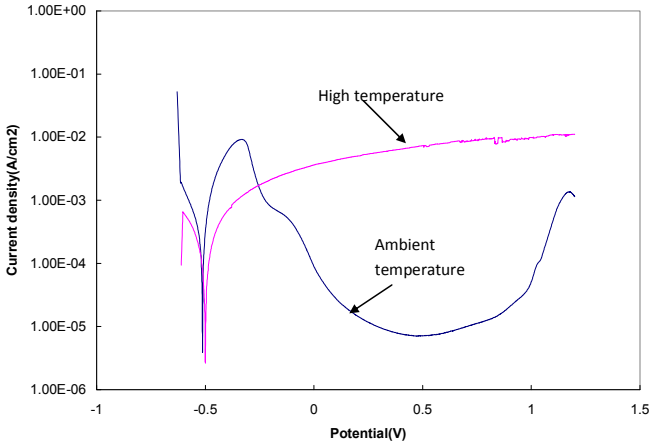

Figure 3. Potentiodynamic polarization curves of SS410 at ambient temperature and 70°C.

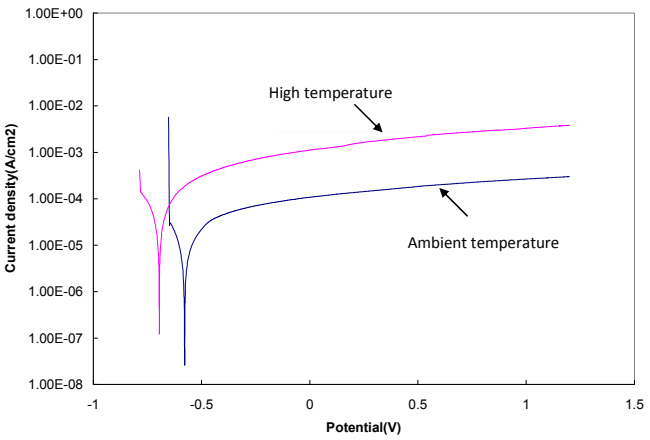

Figure 4. Potentiodynamic polarization curves of Al6061 at ambient temperature and 70°C.

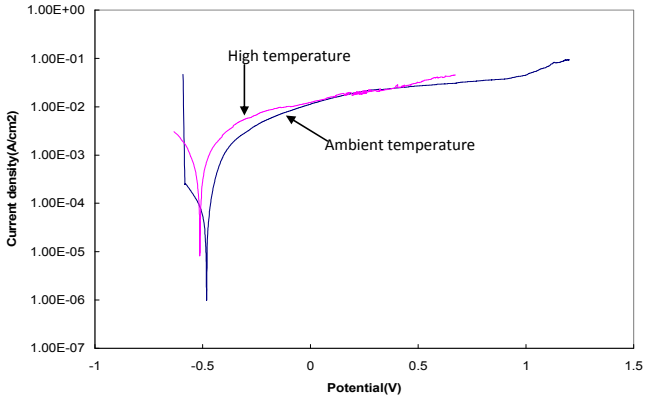

Figure 5. Potentiodynamic polarization curves of A36 steel at ambient temperature and 70°C.

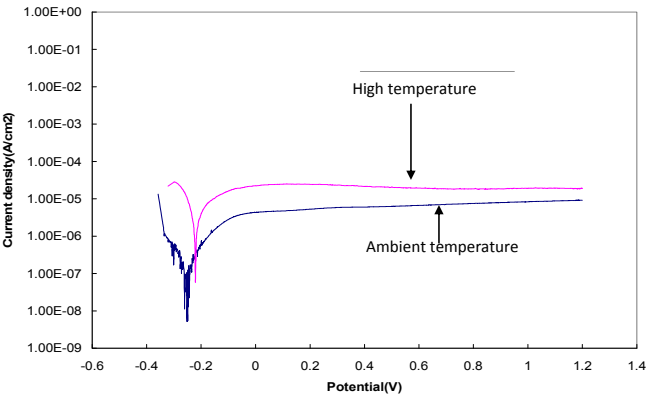

Figure 6. Potentiodynamic polarization curves of Grade 2 Ti at ambient temperature and 70°C.

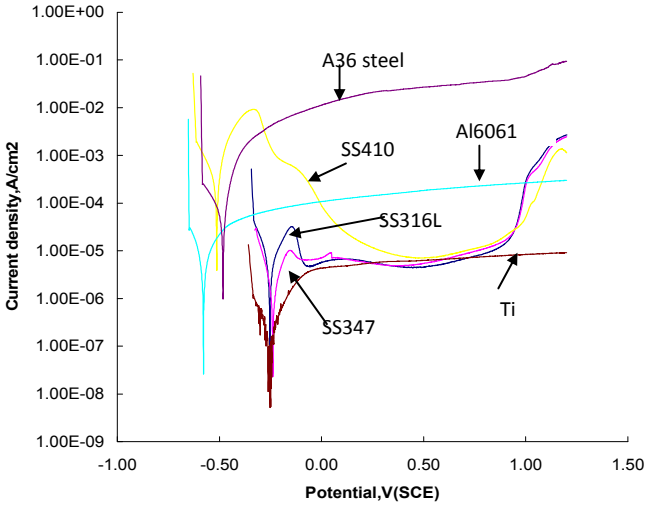

Figure 7. Potentiodynamic polarization curves of the six metals at ambient temperature.

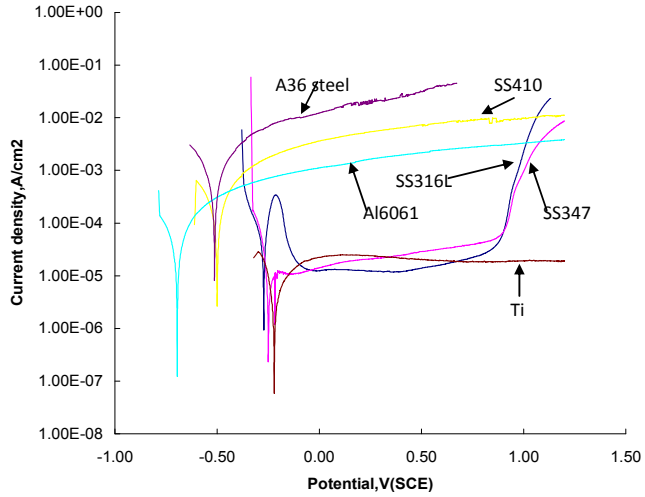

Figure 8. Potentiodynamic polarization curves of the six metals at a high temperature (70°C).

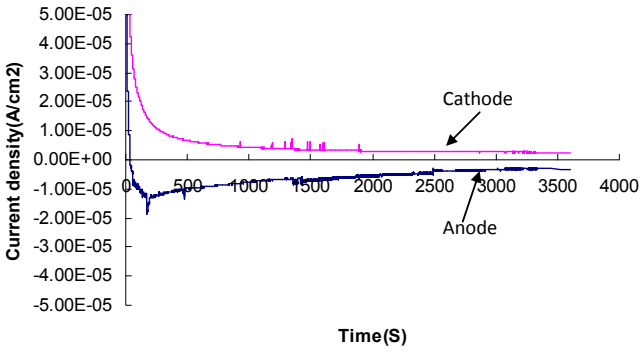

Figure 9. Current density vs. time for SS316L at -0.1V purged with H_2 (anode) and 0.6V purged with O_2 (cathode) at 70°C.

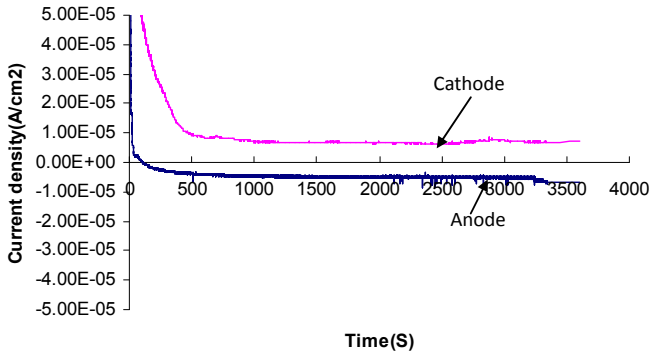

Figure 10. Current density vs. time for SS347 at -0.1V purged with H_2 (anode) and 0.6V purged with O_2 (cathode) at 70°C.

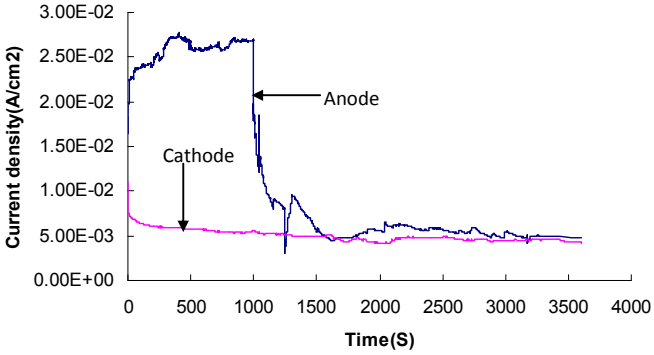

Figure 11. Current density vs. time for SS410 at -0.1V purged with H_2 (anode) and 0.6V purged with O_2 (cathode) at 70°C.

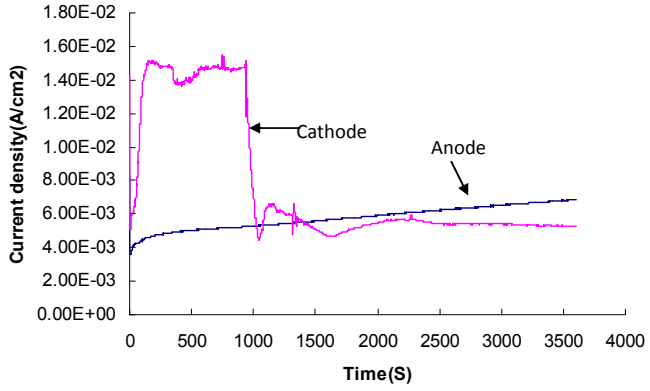

Figure 12. Current density vs. time for Aluminium6061 at -0.1V purged with H_2 (anode) and 0.6V purged with O_2 (cathode) at 70°C.

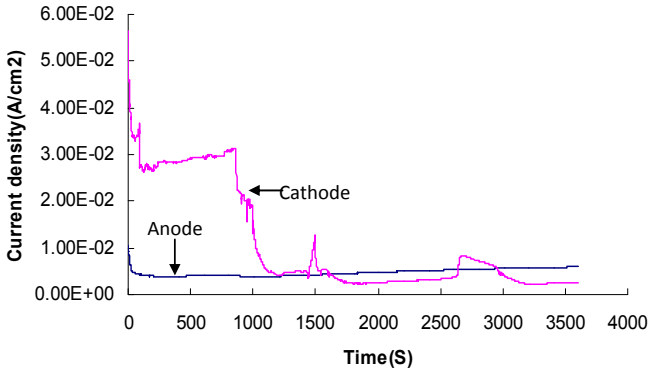

Figure 13. Current density vs. time for A36 steel at -0.1V purged with H_2 (anode) and 0.6V purged with O_2 (cathode) at 70°C.

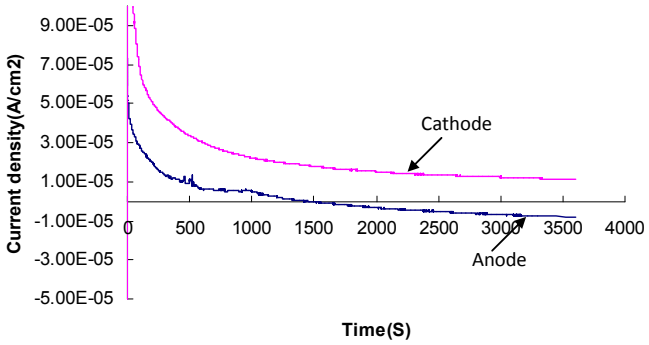

Figure 14. Current density vs. time for Grade2 Ti at -0.1V purged with H_2 (anode) and 0.6V purged with O_2 (cathode) at 70°C.

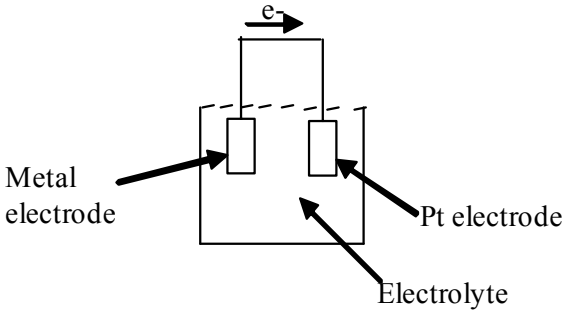

Figure 15. Electron flow during corrosion.

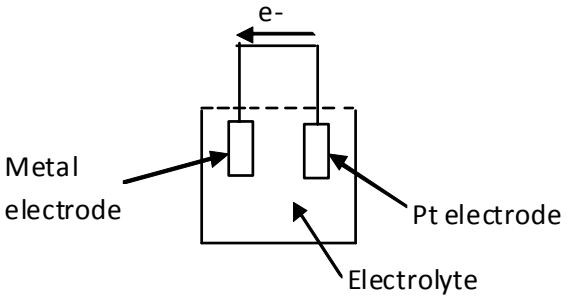

Figure 16. Electron flow when there is no corrosion.

Table4 Anodic and cathodic current densities of the six alloys in simulated PEMFC working conditions

Metal	Anodic current density (A/cm^2)	Cathodic current density (A/cm^2)
SS316	-1×10^{-5}	8×10^{-6}
SS347	-6×10^{-6}	7×10^{-6}
SS410	2.5×10^{-2}, then changes to 4×10^{-3}	4×10^{-3}
Aluminium6061	4×10^{-3}	1.5×10^{-2}, then changes to 4×10^{-3}
ASTM-A36	5×10^{-3}	2.5×10^{-2}, then changes to 4×10^{-3}
Ti	-8×10^{-6}	2×10^{-5}

Table5 Current densities at different applied potentials for SS316L at ambient temperature.

Applied Potential(V)	Current Density(A/cm^2)	Bubbles evolved at electrodes
-0.1	-1.6×10^{-6}	no
-0.2	-2×10^{-5}	no
-0.3	-2×10^{-4}	no
-0.4	-4×10^{-3}	Bubbles at both electrodes
-0.5	-2×10^{-2}	Bubbles at both electrodes

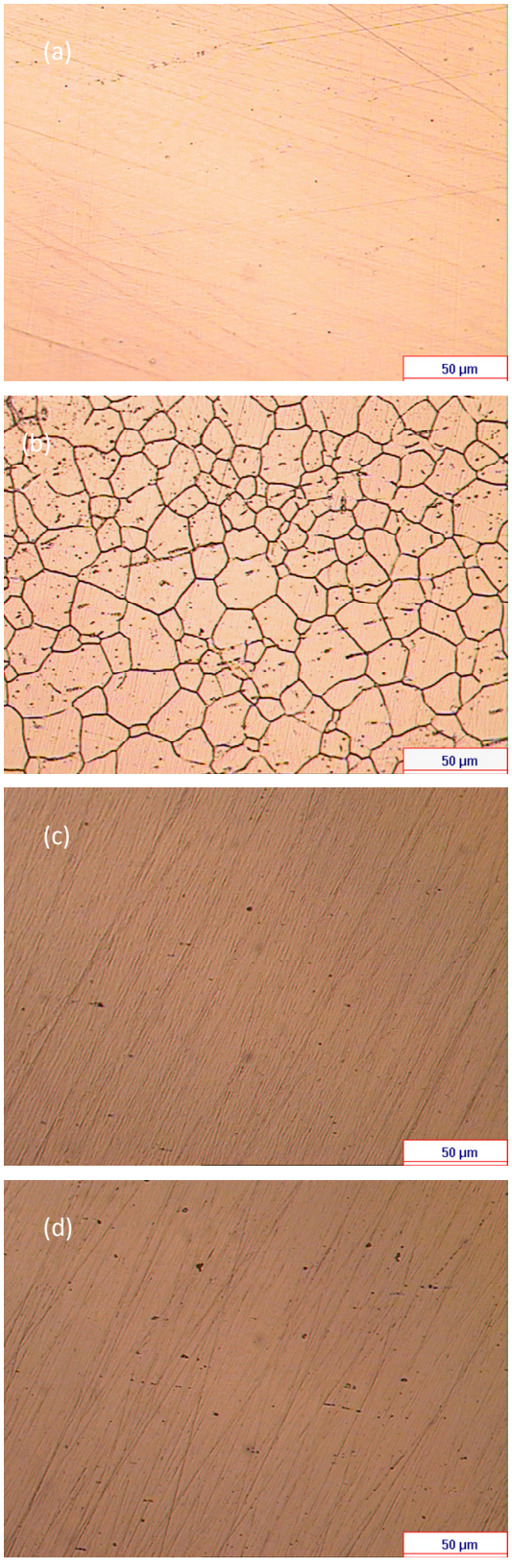

Figure 17. Optical micrographs of surface of SS316L before and after corrosion, (a) before corrosion, (b) after high temperature corrosion, (c) purged with hydrogen, (d) purged with oxygen.

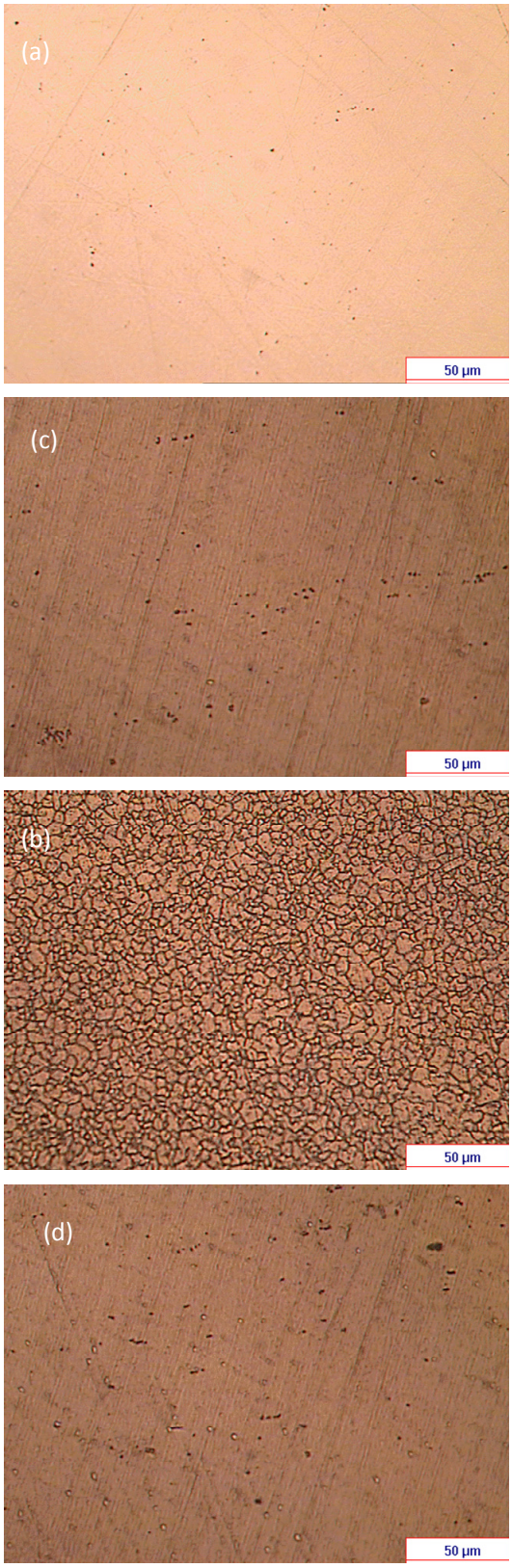

Figure 18. Optical micrographs of surface of SS347 before and after corrosion, (a) before corrosion, (b) after high temperature corrosion, (c) purged with hydrogen, (d) purged with oxygen.

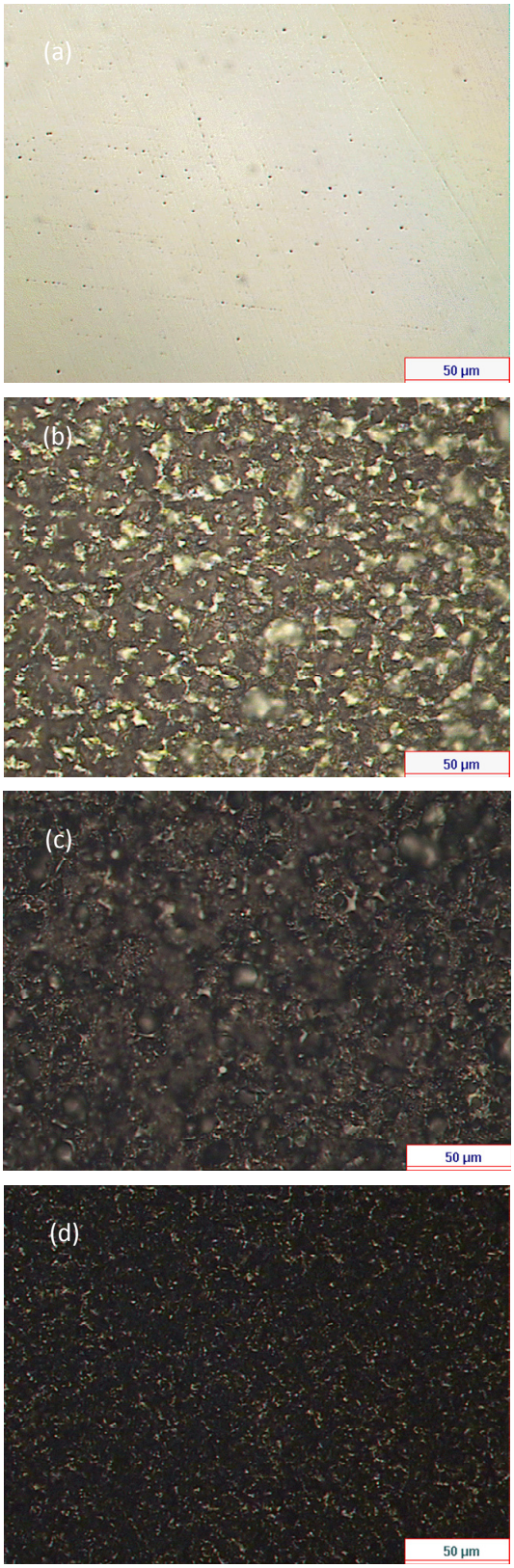

Figure 19. Optical micrographs of surface of SS410 before and after corrosion, (a) before corrosion, (b) after high temperature corrosion, (c) purged with hydrogen, (d) purged with oxygen.

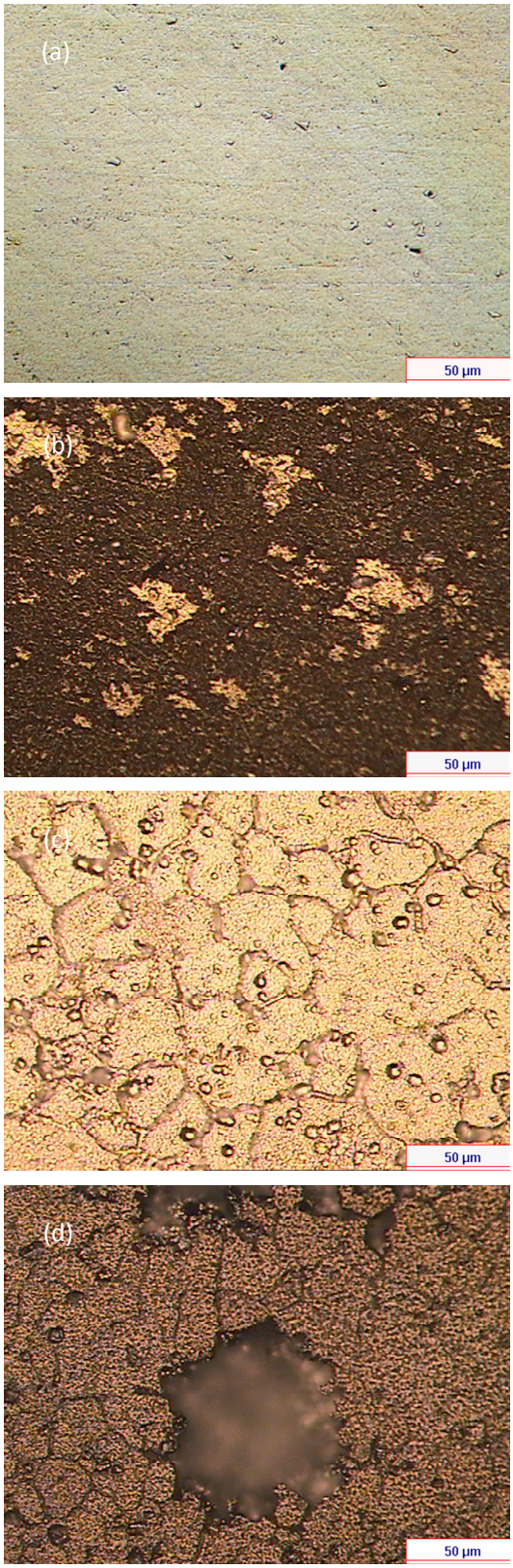

Figure 20. Optical micrographs of surface of Al6061 before and after corrosion, (a) before corrosion, (b) after high temperature corrosion, (c) purged with hydrogen, (d) purged with oxygen.

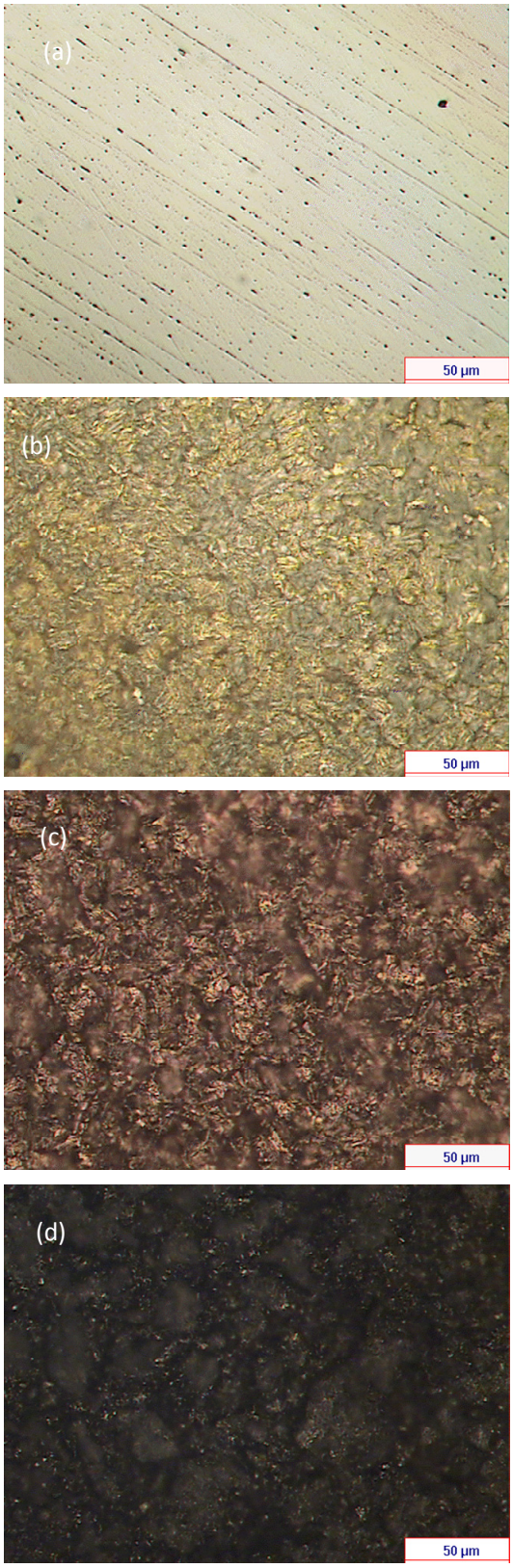

Figure 21. Optical micrographs of surface of A36 steel before and after corrosion, (a) before corrosion, (b) after high temperature corrosion, (c) purged with hydrogen, (d) purged with oxygen.

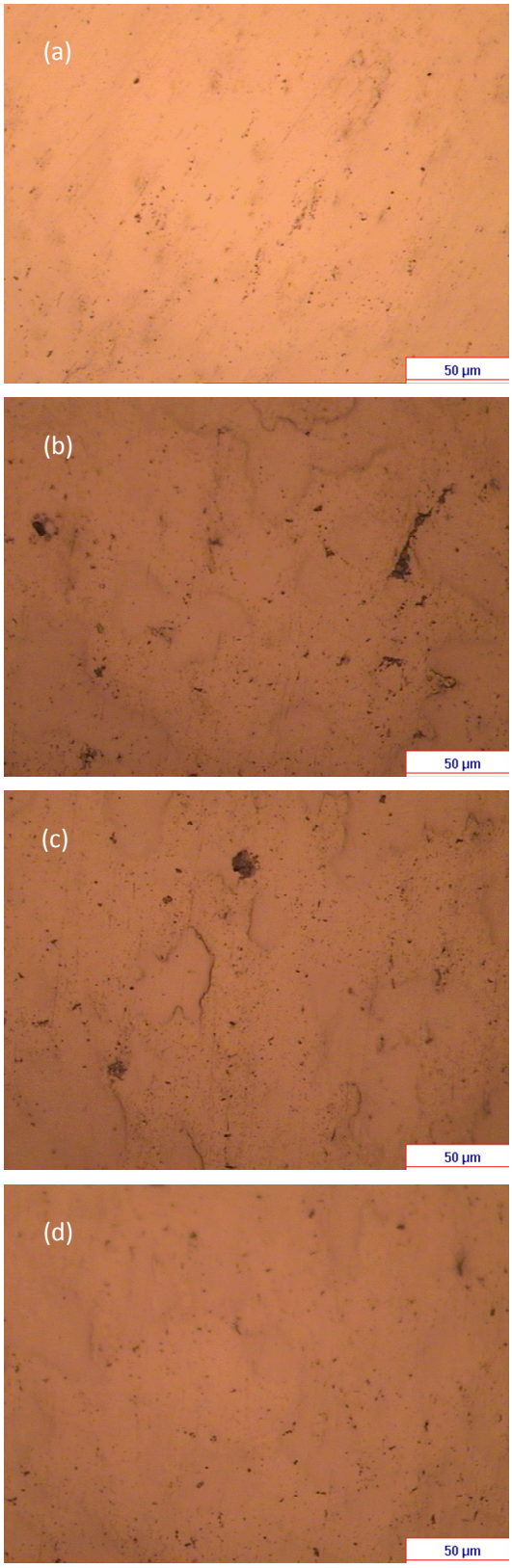

Figure 22. Optical micrographs of surface of Ti before and after corrosion, (a) before corrosion, (b) after high temperature corrosion, (c) purged with hydrogen, (d) purged with oxygen.

then the current density is also lowered. Fig 14 presents the anodic and cathodic corrosion current densities in the simulated anode and cathode environments for Grade 2 titanium. At the anode, the current density is -8×10^{-6}A/cm^2 after 1 hour and at the cathode, the current density is 2×10^{-5}A/cm^2.

Table4 is a summary of all the measured anodic & cathodic current densities. From Table4, we can see that SS316L, SS347 and Ti have a very small current density at both the anode and the cathode. Al6061 and ASTM-A36 have small current densities at the cathode side, but these metals have large current densities at the anode side. SS410 has a larger current density at the anode.

As mentioned before, the current densities of SS316L, SS347 and Ti are negative. The negative current is due to the following reactions:

$$2H^+ + 2e^- \rightarrow H_2 \text{ or } 2H_2O \rightarrow 4H^+ + O_2 + 4e^- \quad \text{Metal electrode} \qquad (1)$$

$$2H^+ + 2e^- \rightarrow H_2 \text{ or } 2H_2O \rightarrow 4H^+ + O_2 + 4e^- \quad \text{Platinum electrode} \qquad (2)$$

When metals corrode at the anode ($M\text{-}2e^- \rightarrow M^{2+}$), the current is positive. This means that there are electrons produced on the metal electrode. In the standard electrode system, the electrons will flow from the metal electrode to the counter electrode (Pt electrode). In this case, the current is positive (Fig15).

However, when the current is negative, electrons should flow from the Pt electrode to the metal electrode (Fig16). On the metal electrode, there is a good supply of H^+ ions. Thus, two reactions including $2H^+ + 2e^- \rightarrow H_2$ and $2H_2O \rightarrow 4H^+ + O_2 + 4e^-$, are possible on the metal electrode. In order to determine which of these reactions was taking place, we did a series of potentiostatic tests at different potentials (-0.1V~-0.5V) for SS316 at ambient temperature. The results are summarized in Table 5.

From Table 5, we can see that the current density increases when the applied potential becomes more negative. When the applied potential reaches -0.4V, there are bubbles formed at both electrodes. The bubbles on the metal electrode are hydrogen and the bubbles on the Pt electrode are oxygen. Even if the current density is -2×10^{-2}A/cm^2, there is no corrosion on the metal surface. Now, we need to determine which reaction occurs on the metal electrode. Because the potential of the $4H^+ + O_2 + 4e^- \rightarrow 2H_2O$ reaction is more positive than that of the $2H^+ + 2e^- \rightarrow H_2$ reaction, the $4H^+ + O_2 + 4e^- \rightarrow 2H_2O$ reaction will take place first. However, the concentration of O_2 is very low because we purge with H_2 for about one hour and there is a high concentration of H^+ ions and the exchange current density of the $2H^+ + 2e^- \rightarrow H_2$ reaction is larger than that of the $4H^+ + O_2 + 4e^- \rightarrow 2H_2O$ reaction. Therefore, we believe, the reaction is mainly $2H^+ + 2e^- \rightarrow H_2$ on the metal electrode.

3.3. Optical microscopy of surfaces of corroded samples

Figs 17-22 are optical micrographs of the surfaces of the six alloys before corrosion, after high temperature potentiodynamic testing, and after potentiostatic tests purged with hydrogen or oxygen. From Figs17 and 18, we can see that the grain boundaries are corroded after high temperature corrosion for both SS316L and SS347. Chromium carbides ($Cr_{23}C_6$) can precipitate at the grain boundaries when the carbon content is over 0.02wt%. When the chromium carbides form at the grain boundaries, they deplete the regions adjacent to the boundaries of chromium so that the chromium level in these areas is decreased below the 12 percent chromium level necessary for passive behaviour. These areas become anodic to the rest of the grain bodies, which are cathodic, thereby creating galvanic couples [19]. When SS316L and SS347 are potentiostatically corroded in the simulated anode conditions, we do not see a corrosion product. This is because the cathodic current provides cathodic protection for the metal. After cathode corrosion, we also can not see a corrosion product on the metal surface. However, this does not mean that there is no corrosion on the metal surface because we observed a corrosion current in the potentiostatic tests. SS410 and A36 steel were uniformly corroded in all three conditions. Alumimium6061 is uniformly corroded after the potentiodynamic tests. However, in the simulated anode and cathode conditions, we could see grain boundary corrosion and pitting corrosion. Moreover, the pitting is more extensive in the simulated cathode condition because the polarization potential is larger. For Grade 2 Ti, in the simulated anode conditions, there is no corrosion. In the simulated cathode conditions and the potentiodynamic test, corrosion is not very severe because the corrosion current is very small. For bipolar plates, the goal for corrosion rate is that it should be less than 1.6×10^{-5}A/cm^2. Strictly this is only applicable to graphite and composite bipolar plates because when these types of bipolar plates are corroded, the product is CO_2 and it will vent with residual H_2 and O_2. From the data that we obtained, it seems that SS316L, SS347 and Grade 2 Ti could be suitable materials for bipolar plates based on the corrosion criteria. However, some researchers [20，21] have reported that metals ions can migrate to the membrane, and that levels as low as 5~10ppm can degrade the membrane performance. Furthermore, PEM fuel cell should have operating lifetimes over 5000h for transportation application [22]. The detailed calculation of metal ion concentration is in the Appendix.

From such a calculation, we can see that the concentration after 5000h is 120ppm for Fe^{2+}, 37ppm for Al^{3+} and 100ppm for Ti^{2+} when the corrosion current density is 10^{-5} A/cm^2. All these concentrations are much higher than 5~10ppm. Therefore, even if the corrosion rate is 10^{-5}A/cm^2, these metals can not meet the requirement that the concentration of metal ions is less than 5~10ppm. Therefore, these metals can probably not be used as bipolar plates, but would require coating to increase their corrosion resistance.

4. CONCLUSIONS

The six different alloys investigated show different corrosion resistance capabilities in the PEM fuel cell environments. SS316L, SS347 and Grade 2 Ti have better corrosion resistances than SS410, Al6061 and A36 steel. In general, the corrosion current increased when the temperature was increased. The corrosion current density is higher in the simulated anode environment than that in the simulated cathode environment for all materials except SS410. The corrosion current densities for SS316L, SS347 and Grade 2 Ti at the anode and cathode are almost the same, but they are positive for the cathode side and negative for the anode side. The positive current is because of the metal corrosion, and the negative current is because the reaction $2H^+ + 2e^- \rightarrow H_2$ can take place on the metal electrode and $2H_2O \rightarrow 4H^+ + O_2 + 4e^-$ takes place on the platinum electrode. There will be no corrosion on the metal

surface at the simulated anode side because the negative current provides cathodic protection for the metal. The differences between the anodic current density and the cathodic current density for SS410, Al6061 and A36 steel are quite large. The anodic corrosion current density is several orders of magnitude higher than the cathodic corrosion current density for both Al6061 and the A36 steel because the polarization potential is increased at the cathode. However, the cathodic corrosion current density is much higher than the anodic corrosion current density for SS410 because SS410 can passivate at the cathode.

The corrosion rate criterion for graphitic or composite bipolar plates, ie less than 1.6×10^{-5}A/cm^2, is not suitable for metallic bipolar plates because metal ions can migrate to the membrane and thereby degrade the membrane performance. Even if the corrosion current is only about 10^{-5}A/cm^2, solution concentrations will be 120ppm for Fe^{2+}, 37ppm for Al^{3+} and 100ppm for Ti^{2+} after 5000h. These metal ion concentrations are much larger than the 10ppm maximum specified. If these metals are directly used as metallic bipolar plates, the concentration of metal ions in solution will reach 10ppm after less than 5000h and the membrane and the fuel cell will begin to degrade. Therefore, these metals must be coated with other materials such as nitrides, carbides or conductive polymers in order to be used as metallic bipolar plates.

5. ACKNOWLEDGEMENTS

The authors wish to thank Drs John Turner and Heli Wang for their helpful comments and suggestions. The research was financially supported by the Natural Sciences and Engineering Research Council of Canada (NSERC) through a Discovery Grant (A4391) awarded to Professor Derek O. Northwood.

6. REFERENCE

[1] A.Hermann, T.Chaudhuri, P.Spagnol. Int.J.Hydrogen Energy 30(2005)1297-1302

[2] H.Tsuchiya, O.Kobayashi. Int.J.Hydrogen Energy 29(2004)985-990

[3] M.Li, C.Zeng, S.Luo, J.Shen, H.Lin, C.Cao. Electrochimica Acta 48(2003)1735-1741

[4] H.Wang, M.A.Sweikart, J.A.Turner. J.Power Sources 115(2003)243-251

[5] H.Wang, J.A.Turner. J.Power Sources 128 (2004)193-200

[6] H. Wang, G. Teeter, and J. Turner. J. Electrochem Soc 152(3)(2005)B99-B104

[7] D.P.Davies, P.L.Adcock, M.Turpin and S.J.Rowen. JAppl Electrochem 30(2000)101-105

[8] M.Li, S.Luo, C.Zeng, J.Shen, H.Lin, C.Cao. Corrosion Science 46(2004)1369-1380

[9] E.A.Cho, U.-S.Jeon, S.-A. Hong, I.-H.Oh, S.-G.Kang. J.Power Sources 14(2005)177-183

[10]S.Lee, C.Huang, J.Lai, Y.Chen. J.Power Sources 131(2004)162-168

[11]N.Cunningham, D.Guay, J.P.Dodelet, Y.Meng, A.R.Hill, and A.S.Hay. J.Electrochem Soc 149 (7)(2002)A905-A911

[12]H.Wang, M.P.Brady, G.Teeter, J.A.Turner. J.Power Sources 138(2004)86-93

[13]H.Wang, M.P.Brady, K.L.More, H.M.Meyer Ⅲ. J.Power Sources 138(2004)79-85

[14]P.L.Hentall, J.B.Lakeman, G.O.Mested, P.L.Adock, J.M.Moore. J.Power Sources 80(1999)235-241

[15]K.M.El-Khatib, M.O.A.Helal, A.A.El-Moneim and H.Tawfik. Anti-Corros Method M 51(2004)136-142

[16]S.Lee, C.Huang, Y.Chen. J Mater Process Tech 140(2003)688-693

[17]D.R.Hodgson, B.May, P.L.Adcock, and D.P.Davies. J.Power Sources 96(2001)233-235

[18]W.F.Smith, Foundations of Materials Science and Engineering, New York, Third Edition, McGraw-Hill, 2004, P497

[19]W.F.Smith, Foundations of Materials Science and Engineering, New York, Third Edition, McGraw-Hill, 2004, P702

[20]L.Ma, S.Warthesen, D.A.Shores. J New Mater Electrochem Syst 3(2000)221-228

[21]M.P.Brady, K.Weisbrod, I.Paulauskas, R.A.Buchanan, K.L.More, H.Wang, M.Wilson, F.Garzon, L.R.Walker, Scripta Mater 50(2004)1017-1022

[22]R.G.Rajendran. MRS Bulletin 30(2005)587-590

APPENDIX:

Calculation of metal ion concentrations for PEM fuel cell after 5000h operation

Suppose $i_{corr}=10^{-5}$A/cm^2

The electrode area is 2.25 cm^2

$I=iA=10^{-5}\times2.25=2.25\times10^{-5}$A

$C=It=2.25\times10^{-5}\times5000=0.1125$Ah

0.1125/26.8= 0.004198F

Suppose Fe change to Fe^{2+}, $0.004198\times29/58=0.002099$mol

Al changes to Al^{3+}, $0.004198\times9/27=0.0014$mol

Ti changes to Ti^{2+}, $0.004198\times24/48=0.002099$mol

The volume of solution is about 0.1L

Suppose 10 percent of these metal ions will remain in the PEM fuel cell stack.

Wt of Fe^{2+} in the solution after 5000h is

$(2.099\times10^{-3}\times58/0.1)\times0.1=1.2\times10^{-1}$g/L≈120ppm

Wt of Al^{3+} in the solution after 5000h is

$(1.4\times10^{-3}\times27/0.1)\times0.1=3.7\text{x}10^{-2}$g/L≈37ppm

Wt of Ti^{2+} in the solution after 5000h is

$(2.099\times10^{-3}\times48/0.1)\times0.1=1\text{x}10^{-1}$g/L≈100ppm